SCIENTIFIC REPORTS

OPEN

SUBJECT AREAS:
MATERIALS FOR ENERGY AND CATALYSIS
TWO-DIMENSIONAL MATERIALS
NANOSCALE MATERIALS
BATTERIES

Received
18 March 2013

Accepted
25 June 2013

Published
9 July 2013

Correspondence and requests for materials should be addressed to H.Y.Y. (yanghuiying@sutd.edu.sg)

Self-assembly of hierarchical MoS_x/CNT nanocomposites (2<x<3): towards high performance anode materials for lithium ion batteries

Yumeng Shi[1], Ye Wang[1], Jen It Wong[1], Alex Yuan Sheng Tan[1], Chang-Lung Hsu[2,3], Lain-Jong Li[2,4], Yi-Chun Lu[5] & Hui Ying Yang[1]

[1]Pillar of Engineering Product Development, Singapore University of Technology and Design, Singapore 138682, Singapore, [2]Institute of Atomic and Molecular Sciences Academia Sinica, Taipei 10617, Taiwan, [3]Department of Materials Science & Engineering, National Chiao Tung University, HsinChu 300, Taiwan, [4]Department of Physics Natonal Tsing Hua University, HsinChu 300, Taiwan, [5]Department of Mechanical and Automation Engineering, The Chinese University of Hong Kong, Hong Kong SAR, China.

Two dimension (2D) layered molybdenum disulfide (MoS_2) has emerged as a promising candidate for the anode material in lithium ion batteries (LIBs). Herein, 2D MoS_x ($2 \leq x \leq 3$) nanosheet-coated 1D multiwall carbon nanotubes (MWNTs) nanocomposites with hierarchical architecture were synthesized via a high-throughput solvent thermal method under low temperature at 200°C. The unique hierarchical nanostructures with MWNTs backbone and nanosheets of MoS_x have significantly promoted the electrode performance in LIBs. Every single MoS_x nanosheet interconnect to MWNTs centers with maximized exposed electrochemical active sites, which significantly enhance ion diffusion efficiency and accommodate volume expansion during the electrochemical reaction. A remarkably high specific capacity (i.e., > 1000 mAh/g) was achieved at the current density of 50 mA g^{-1}, which is much higher than theoretical numbers for either MWNTs or MoS_2 along (~372 and ~670 mAh/g, respectively). We anticipate 2D nanosheets/1D MWNTs nanocomposites will be promising materials in new generation practical LIBs.

Advanced energy storage technology is the key to manage the energy supply and demand. Lithium ion batteries (LIBs) have attracted increasing research interests and become one of the main power sources for portable electronic devices and electric vehicles due to its high energy densities, no memory effect, and good cycling stability compared to other alternatives[1]. In commercial LIBs, graphite and lithium metal oxides are commonly employed as the negative (anode) and positive (cathode) electrode materials, respectively. Lithium is the lightest metal that delivers high energy density per electron with a theoretical electrochemical capacity of Li to Li^+ is 3860 mAh/g[2]. However, further advancements in the state-of-the art LIBs are still bottlenecked by the limitation in the anode materials associated with limited capacity (i.e., graphite, ~372 mAh/g), lack of shape flexibility and low ion/electron conductivity[3,4]. In the past few years, substantial research efforts have been devoted in developing high performance LIBs electrodes. Various carbon nanomaterials, such as one dimension (1D) carbon nanotubes (CNTs)[5,6], two dimension (2D) graphene nanosheets[7,8], three dimension (3D) graphene foam[9,10], have all been investigated as the anode materials in reversible storage of Li^+, due to their outstanding electronic conductivities, high charge mobilities and large specific surface areas. As one of the crystalline form of carbon, 1D CNTs has high electric conductivity, good mechanical property, chemical stability and reversible redox reaction capability, which makes it a promising candidate as lithium insertion hosts for LIBs.

The nanostructured multifunctional heterostrucutres have been proved to work synergistically with both high capacity and good cyclability[11–14]. Molybdenum disulfide (MoS_2), an inorganic graphite analogue, belongs to the layered transition-metal dichalcogenide (LTMDs) family. The weak van der Waals interaction between MoS_2 layers allows the Li^+ ions to diffuse without a significant increase in volume expansion and prevent the pulverization problem of active materials caused by the repeatly lithiation and delithiation process. The promising potential of MoS_2 serving as an anode materials for LIBs is widely reported in the literature due to its attractive specific capacity[15–21]. Theoretically the conversion reaction between Li ions and MoS_2 leads to four moles of

lithium incorporation per mole of MoS_2 accounting for 670 mA h g^{-1} lithium storage capacity that is ~1.8 times higher than the graphite electrode[20]. With all these significant advantages, MoS_2 has attracted lots of research interests and became a promising material as an anode material in LIBs[17–19]. Various methods have been reported for the synthesis of MoS_2 including the gas-phase reaction of MoO_3 with H_2S or S vapor[22,23], thermal decomposition of ammonium thiomolybdate[24,25], and solvent thermal method[26,27].

The solvent thermal process is an important wet chemistry synthesis method and has been widely used to prepare various nanomaterials or nanocomposites. It has been reported CNTs favored the growth of the tubular MoS_2 on the surface of carbon nanotube side walls and promoted the formation of tubular MoS_2 layers with high crystallinity[27–29], CNTs/MoS_2 composites have also been prepared by the simple solvothermal method[30,31]. For example, tubular MoS_2 layers coating on CNTs were synthesized by the hydrothermal reaction between Na_2MoO_4 and $CS(NH_2)_2$ with the presence of CNTs[12]. The surface area of MoS_2 is limited by the surface area of CNTs. Nevertheless, when aqueous solvent is used, CNTs need to be treated by refluxing in high concentrated strong acid in order to improve the wetting between CNTs and MoS_2 precursor[28]. This acidic treatment will introduce defects in CNTs and negatively affect the electrical properties of CNTs. MoS_2/CNTs with a design of 2D MoS_2 nanoflakes surrounded by a coating of CNTs was synthesized by using Na_2MoO_4 and KSCN as reactant and ethylene glycol as solvent in the presence of CNTs[27]. These composites show higher capacity and improved cycling stability compared to pure MoS_2. The MoS_2 nanoflakes synthesized are relatively thick and randomly attached to CNTs, which causes a continues capacity fading during cycles[27]. Wang *et al.* prepared MoS_2 overlayers supported on coaxial CNTs by wet-chemistry process and studied the reversible lithium-storage behaviors of this composite[32]. A reversible capacity of 400 mAh/g was achieved; however this value is much smaller than the non-coaxial MoS_2/CNTs composite.

Results

Herein, we report a unique MoS_x/CNTs ($2 \leq x \leq 3$) nanostructure synthesized by simple solvent thermal method at low temperature (200°C) using $(NH4)_2MoS_4$ as single reactant and N,N-dimethylformamide (DMF) as solvent in the presence of MWNTs. The synthesized MoS_x/MWNTs composites are different from the previous report for MoS_2 sheath/CNT-core nanoarchitecture[32], the MoS_x layers are not confined to the MWNTs surface, but extend the layered structure out of the cylindrical tubules (as shown in Figure S1). To understand the forming of hierarchical architecture, the morphology and lattice structure of as prepared MoS_x/MWTNs composite was compared with the samples treated under elevated temperature. Figure 1 (A), (B) show the TEM images of MoS_x coated MWNTs prepared by the solvent thermal method. The HRTEM in Figure 1 (B), gives a close-up view of the MoS_x branch attached on MWNTs surface. The inset shows a fast Fourier transform (FFT) pattern taken from the marked area in Figure 1 (B). The HRTEM and FFT results indicate the semi-crystalline nature of the MoS_x layers. As seen in Figure 1 (C) and (D) MoS_2 sheath/CNT-core nanoarchitecture was obtained by thermal annealing at 800°C under Ar protecting environment. The two layered spacing can be identified to be around ~0.62 and ~0.34 nm, which are in good consistence with the value for MoS_2 layers and the lattice spacing between the graphitic planes of MWNTs. Figure 1 (E) and (F) compare the Raman spectra taken from the as obtained MoS_x/MWNTs samples and thermal treated MoS_2 sheath/CNT-core nanocomposites. The Raman Peaks at around 1347 and 1576 cm^{-1} belong to MWNTs. The G′ band of MWNTs locates at 2686 cm^{-1}. The Raman Peaks of MoS_2 appear at 376 and 402 cm^{-1}. It was also found that the Raman signature of MoS_2 dramatically increased after thermal annealing, which suggests the formation of highly crystallized MoS_2 layers. This is agreed with the result of HRTEM.

X-ray photoelectron spectroscopy (XPS) was used to investigate the chemical states of Mo and S in the MoS_x/MWNTs nanocomposites. Figure 2 displays the XPS characterization of the samples before and after thermal annealing at 800°C under Ar protecting environment. The high-resolved XPS spectra shows the binding energies of Mo 3d 3/2, Mo 3d 5/2, S 2p ½ and S 2p 3/2 peaks in the thermal annealed MoS_x/MWNTs are located at 232.4, 229.2, 163.3 and 162.1 eV, respectively, indicating that Mo^{4+} existed in the annealed MoS_x/MWNTs[32]. The stoichiometric ratio of S:Mo estimated from the respective integrated peak area of XPS spectra is ~2.125 suggesting the structure is close to MoS_2. For the as prepared MoS_x/MWNTs two broaden peaks centered at ~232.5 and ~228.9 eV, in addition to the XPS peaks for MoS_2 structure, other sets of peaks are also observed. The higher energy shift of Mo $3d_{3/2}$ and $3d_{5/2}$ doublet are associated with higher valence states. The observation of Mo $3d_{3/2}$ and Mo $3d_{5/2}$ peaks at 233.6 and 230.5 eV with separation energies close to 3.1 eV can be attributed to the presence of Mo^{5+} ions[33,34]. For the non-annealed MoS_x/MWNTs the S 2p spectra can be interpreted in terms of two doublets, with S 2p3/2 binding energies of 161.7 and 163.2 eV. Compared to the thermal annealed samples, the additional S 2p1/2 and 2p3/2 energies located at 164.3 and 163.2 eV can be assigned to the binding energies of apical S^{2-} or bridging disulfide S_2^{2-} ligands. The S 2p spectrum that can be fit with two S 2p doublets, which is similar to those of amorphous MoS_3[35,36]. The presence of bridging apical S^{2-} or bridging S_2^{2-} is in good consistence with the TEM analyses in Figure 1 (B), which reveals that the MoS_x obtained are basically semicrystalline. Furthermore, the S/Mo elemental ratio estimated from the integrated peak area of XPS spectra is ~3.0 which also suggests the as grown MoS_x is stoichiometrically close to MoS_3. The thermal decomposition of $(NH4)_2MoS_4$ is accompanied by molybdenum-sulfur redox processes, which include the oxidation of S^{2-} ligands of the MoS_4^{2-} anion and the reduction of Molybdenum metal from Mo^{VI} to Mo^{IV}, and various thermal decomposition intermediate may exist[37]. The XPS results confirm the presents of MoS_3 while the Raman spectra from the as prepared samples show smaller but visible Raman Peaks of MoS_2 at 376 and 402 cm^{-1} (as shown in Figure 1(E)). Therefore, the exact phase of the MoS_x/MWNTs compound is suggested to be a mixture of MoS_2 and MoS_3.

The growth mechanism of MoS_x/MWNTs layered structures were also investigated by varying the Mo/Carbon ratio in the precursor. Figure 3 (A), (B) and (C) show the TEM images of typical MoS_x/MWNTs composites prepared with Mo/Carbon ratio of 1 : 40, 1 : 20 and 1 : 10. Figure 3 (D) proposes the growth mechanism of the MoS_x/MWNTs composites. With limited amount of MoS_x precursor the MoS_x forms small segments on the sidewall of MWNTs. The hierarchical structure of MoS_x forms and the MoS_x layer structure extruding from the sidewall of MWNTs with the increase of Mo/C ratio. For the high concentration precursor, the MoS_x layers form uniformly on MWNTs. It has been reported CNTs favored the growth of the tubular MoS_2 on the surface of carbon nanotube side walls and promoted the formation of tubular MoS_2 layers with high crystallinity[27,28], therefore at elevated temperate the MoS_x converted to MoS_2 and form MoS_2 sheath/CNT-core nanoarchitecture[32].

Discussion

Compared to the conventional MoS_2/MWNTs structure, the novel MoS_x/carbon composite has a three dimensional (3D) hierarchical structure, where the 1D multi wall carbon nanotube (MWNTs) as back bones, while the 2D MoS_x layers grown on the surface of MWNTs with a partially free standing branch like feature, which provide a large surface area of the active material to accommodate Li^+. The hierarchical structure of MoS_x/CNTs, could effectively combine the merits of the good electrical conductivity of CNTs and

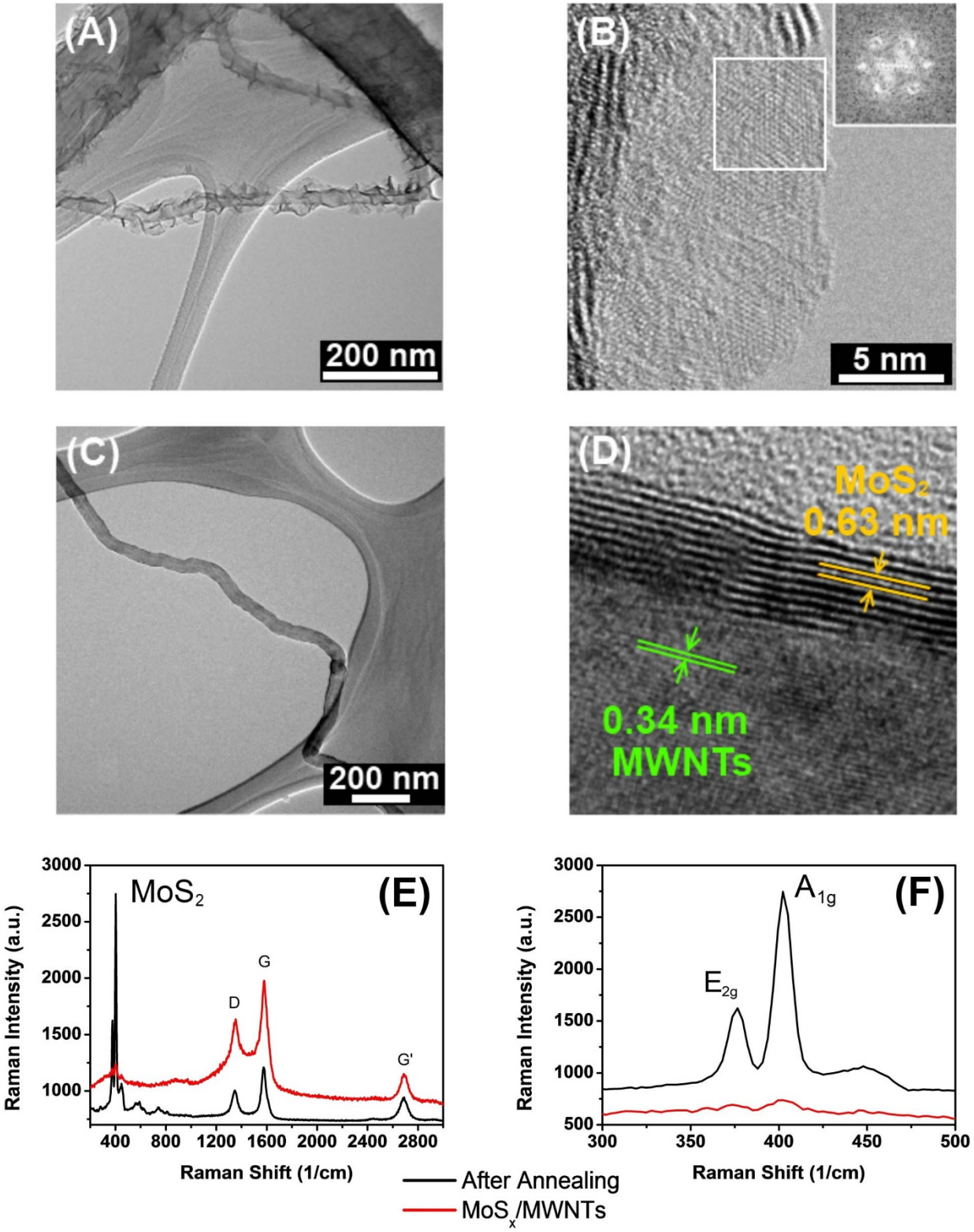

Figure 1 | (A) and (C) Low-magnification TEM image of MoS_x/MWNTs with hierarchical nanostructure and MoS_x/MWNTs after annealing at 800°C under Ar protection, (B) and (D) HRTEM images of a free standing monolayer MoS_x and the side wall of the composite after annealing. Inset in Figure 1 (B) shows the FFT pattern taken from the marked area. (E) Raman spectra of the MoS_x/MWNTs. Figure 1 (F) compares the magnified Raman signature of ta prepared MoS_x/MWTNs and the one after annealing.

excellent electrochemical performance of individual MoS_x layer throughout cycling. Due to the excess of sulphur in MoS_x an increased layer distance of S–Mo–S can be expected, which results in less strain and smaller intercalation barrier of Li ions. Meanwhile, the CNTs used in this work have a long tube length, which creates large internal voids in the composites that could absorb and buffer the mechanical stress which caused by the local volume variation during lithium insertion and extraction.

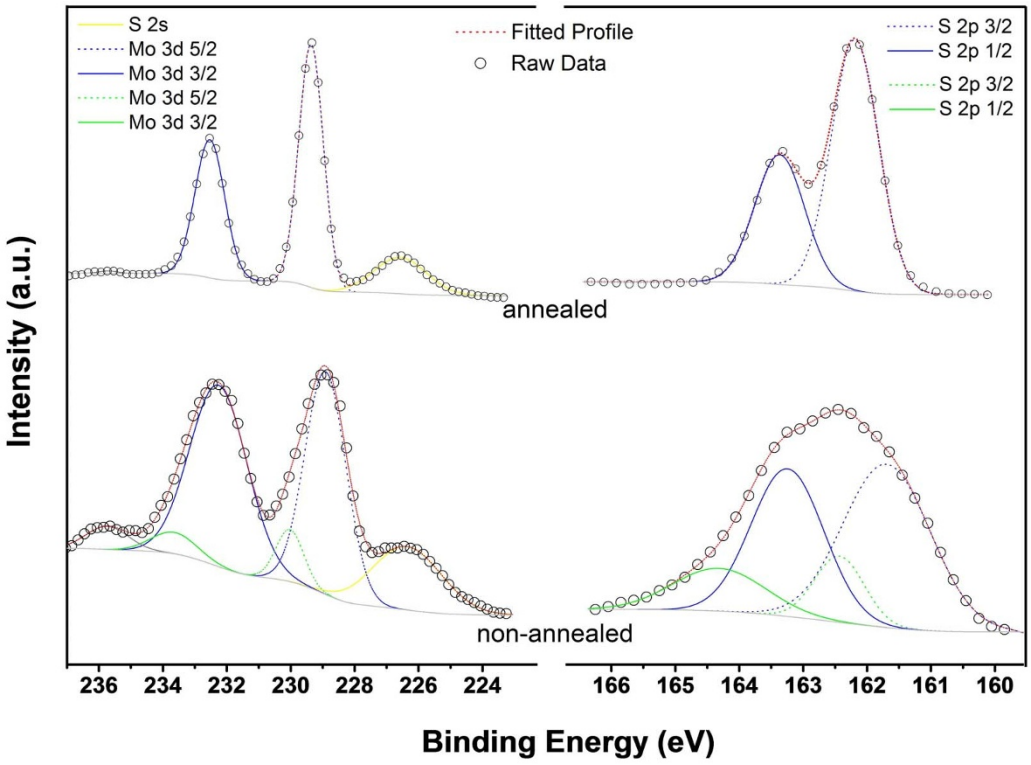

Figure 2 | Chemical composition analysis by X-Ray photoemission spectroscopy (XPS) for Mo and S. The lower and upper cures display the corresponding spectrum taken from the as obtained and 800°C annealed MoS_x/MWNTs samples respectively.

Considering the electrodes with special hierarchical nanocomposites are advantageous to LIBs, we investigate the lithium storage properties of as-prepared MoS_x/MWNTs using half-cell configuration. Figure 4 shows the electrochemical performance of MoS_x/MWNTs as anode materials. Figure 4 (A) illustrates the first, second, fifth and tenth discharge/charge voltage profiles of the MoS_x/MWNTs composite electrode in the voltage range of 0.01 to 3 V (vs. Li/Li^+). During the first discharge, the initial discharge capacity between 2.0 to 1.5 V can be attributed in part to the reaction of residual carbon (MWNTs) surface functional group[38] and in part to lithium insertion into the MoS_x/MWNTs composites forming Li_nMoS_x ($0 < n < 4$)[39], according to the reaction $MoS_x + nLi^+ + ne^- \rightarrow Li_nMoS_x$[27,40]. We note that it is previously proposed that a better formulation for MoS_3 would be $Mo^V_2(S_2^{2-})(S^{2-})_4$, therefore, the reduction of sulfur during initial discharge can also be considered here[39]. Following this, the capacity between 1.0 to 0.5 V can be attributed to the conversion reaction process $MoS_x + 2xLi^+ + 2xe^- \rightarrow Mo + xLi_2S$[41–43]. The metal sulfide reacts with lithium ions forming metal nanoparticles and insoluble Li_2S matrix[20]. It was argued that the nanosized metal particles promote the reversible reaction which is responsible for the reversible lithium-storage capacity, therefore the phase segregation of transition metals should be limited in order to improve the cycling stability[32]. The sloping plateau at the lower voltage region (below 0.5 V) includes the contribution from

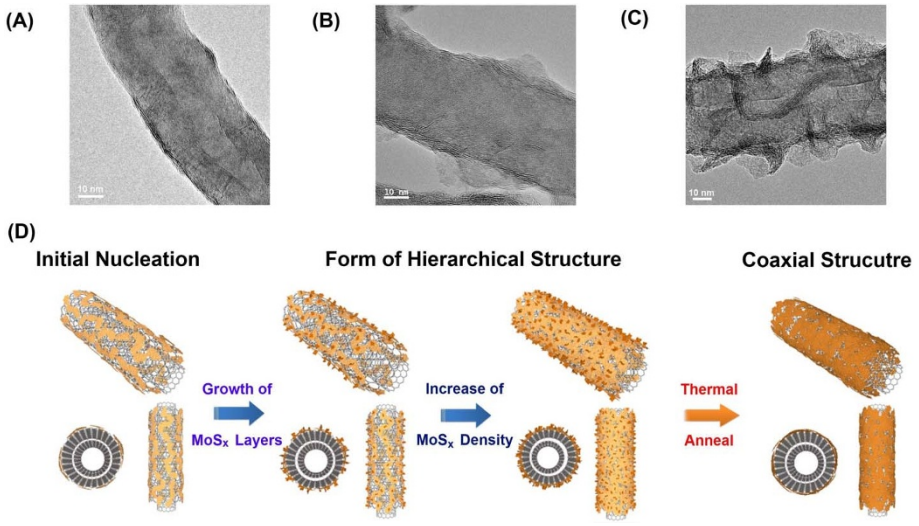

Figure 3 | (A),(B) and (C) Low-magnification TEM images of MoS_x/MWNTs with synthesized with increasing MoS_x/MWNTs ratio (1 : 40, 1 : 20, 1 : 10), (D) shows the proposed growth mechanism for forming MoS_x/MWNTs hierarchical structure.

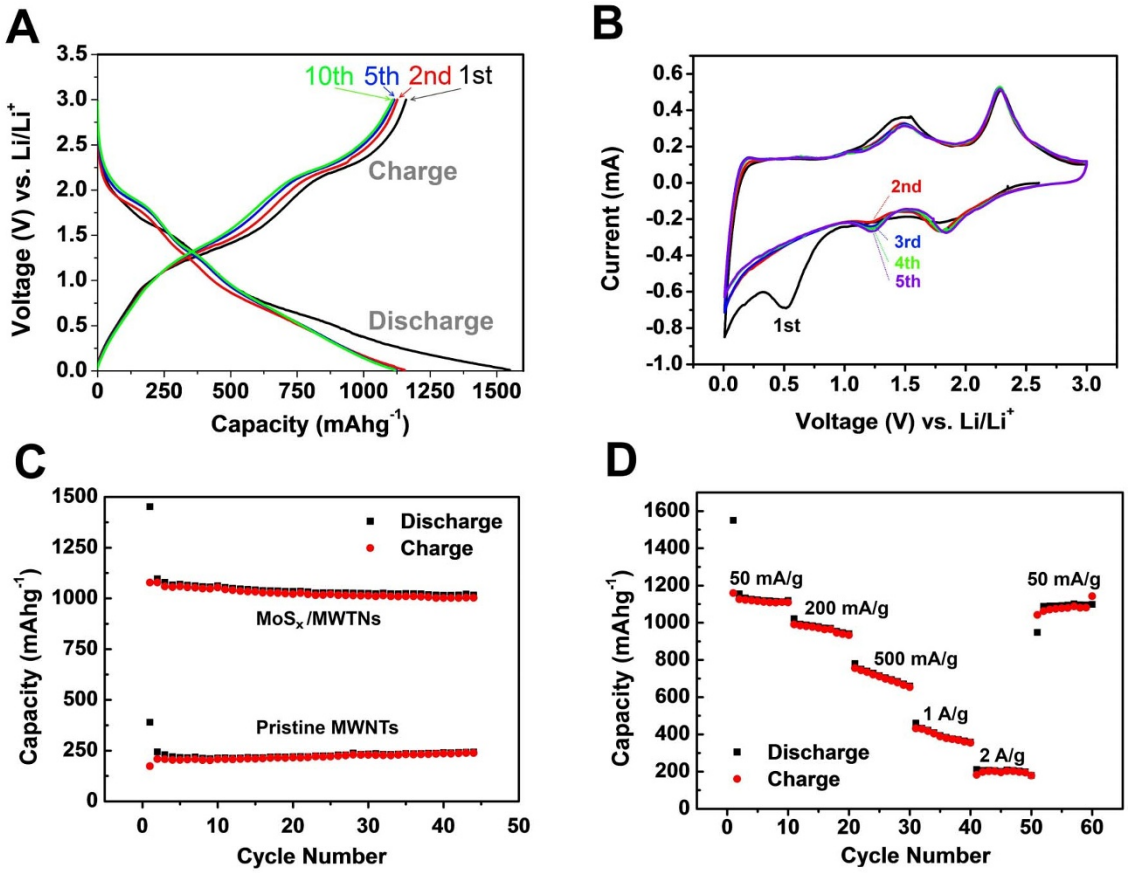

Figure 4 | (A) Voltage profiles of MoS_x/MWNTs charged-discharged at 50 mA g^{-1}, (B) Representative cyclic voltammograms of MoS_x/MWNTs composite for the first 5 cycles at a scan rate of 0.5 mVs^{-1} between 0.01 V and 3 V. (C) comparison of cycling stability between MoS_x/MWNTs and MWNTs charged-discharged at 50 mA g^{-1}), and (D) Rate capability of MoS_x/MWNTs charged and discharged at various current densities.

the formation of a solid electrolyte interface (SEI) and the gel-like polymeric layer on the surface of the active materials[44]. In the subsequent charge process, a plateau at ~1.3 V and the sloping region above 2.2 V are attributed to the oxidation of Mo particles to MoS_x and the oxidation of Li_2S to form S, respectively[42,45,46]. We note that lithium extraction from the Li_nMoS_x phase should also be considered here[27,39,40]. The initial discharge and charge capacities are found to be 1549 and 1159 $mAhg^{-1}$, respectively. (with a Coulombic efficiency of 74.8%).The irreversible capacity loss of approximately 25.1% in the 1st cycle can be mainly attributed to the irreversible processes including the electrolyte decomposition and inevitable formation of the SEI, which have been observed for nanosized anode materials[47]. During the 2nd cycle, the discharge capacity decreases to 1154 mAh/g with a corresponding charge capacity of 1126 mAh/g, leading to a much higher Coulombic efficiency of 97.5%. This value further increased to 99.6% in the 5th cycle and still maintained above 98.6% at the 10th cycle. To further clarify the electrochemical process of the MoS_x/MWNTs composite, cyclic voltammograms (CV) measurement of the first three cycles in the voltage range of 3.0 – 0.01 V with a scan rate of 0.1 mVs^{-1} was shown in Figure 4 (B). In the first cycle a very small reduction peak at ~1.80 V was found, which can be related to the reaction of residual carbon surface functional group[38], in part to lithium insertion into the MoS_x structure forming Li_nMoS_x[39], and the reduction of traced sulfur[39]. A pronounced reduction peak at ~0.50 V was observed in the first cycle, however for the subsequent cycles, the peak at ~0.50 V disappeared. This process has been attributed to the decomposition of MoS_x into Mo nanoparticles embedded in a Li_2S matrix through the conversion process[42,43]. Upon the anodic scan, the oxidation peak at ~1.5 V can be in part attributed to the oxidation of Mo to MoS_2 followed by a anodic peak at 2.3 V associated with the oxidation of Li_2S into S[42,43,45]. In addition, lithium extraction from Li_nMoS_x could contribute to these anodic processes depending on the stoichiometry of the $LinMoS_x$[39]. During the 2nd CV scan, a pair of reduction peak at ~1.3 V and ~1.80 V together with two corresponding oxidation peaks at ~ 1.5 and 2.3 V for the MoS_x/MWNTs composite became distinct. The reduction peak at ~1.3 V can be related to the intercalation of Li^+ into the MoS_x lattice While, the oxidation peaks at ~1.48 V and 2.28 V correspond to the extraction of Li^+ from Li_nMoS_x lattice and the oxidation of Li_2S, respectively[40].

Figure 4 (C) shows the cycling stability of the MoS_x/MWNTs electrode compared to the pristine MWNTs. The specific capacity of the MoS_x/MWNTs composite with a Mo/C molar ratio of 1 : 1 is above 1000 mAh/g which is more than 4 times larger than the pristine MWNTs electrodes under current density of 50 mA/g. The specific capacities of MoS_x/MWNTs composites with various Mo/C molar ratios are shown in supporting information Figure S2. Figure 4 (D) shows the rate capability of the MoS_x/MWNTs composites at various current densities. The electrode shows the 10th-cycle discharge capacities of 1119, 904, 659, 358 and 197 $mAhg^{-1}$ at current densities of 50, 200, 500, 1000 and 2000 mAg^{-1}, respectively. Even at a very high current density of 1000 mAg^{-1}, the composite electrode can still deliver a capacity of 358 $mAhg^{-1}$, which is comparable with the theoretical capacity of graphite (372 mAh g^{-1}). Furthermore, after the current density returns from 2000 mAg^{-1} to 50 mAg^{-1}, the specific capacity of MoS_x/MWNTs electrode can recover to 1087 $mAhg^{-1}$ and remain 1098 $mAhg^{-1}$ after 10 cycles. Our MoS_x/CNTs have shown a remarkably high reversible specific capacity (i.e., > 1000 mAh/g) at the current density of 50 mA g^{-1}, which is much larger than the "theoretical" capacity value of MoS_2

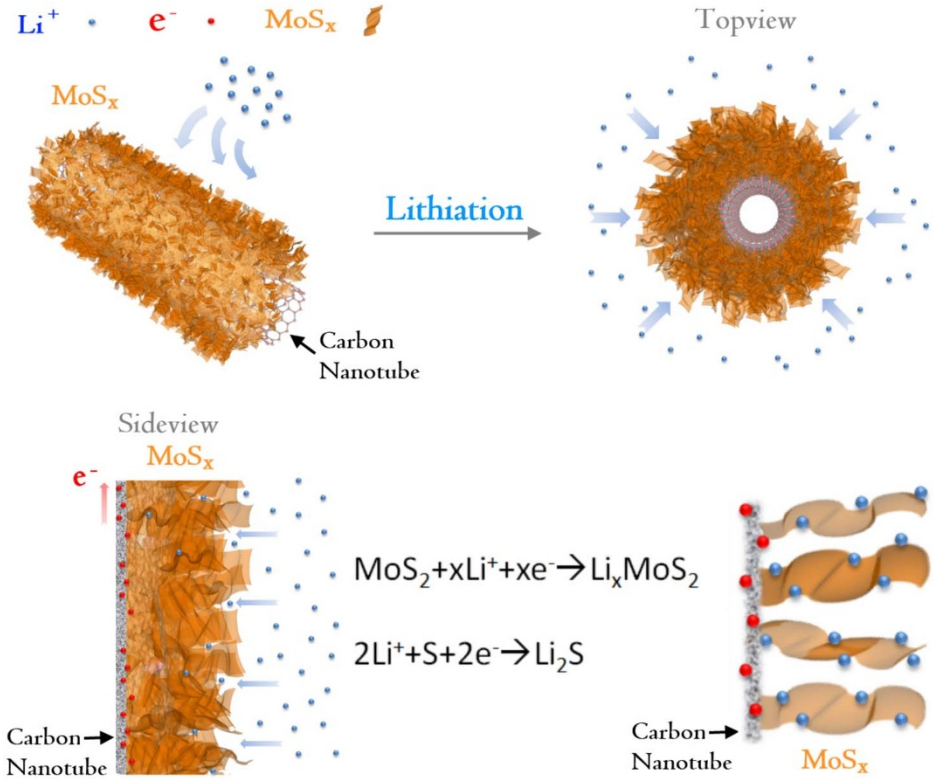

Figure 5 | Schematic illustration of the diffusion of electron and Li. The Li ion can diffuse into the hierarchical MoS_X/MWNTs nanocomposites easily from the open space between neighboring. Hierarchical structures enhance the contact area, shorten the Li ion diffusion length in the nanosheets, and ensure that Li and electron diffuse with little resistance.

(670 mAh/g assuming 4 lithium ions per MoS_2) and CNTs along. We note that specific capacity of MoS_2 higher than 670 mAh/g is well-documented in the literature[45,48,15]. It was shown that MoS_2 can take up to 8 lithium ions with major capacity between 0.01 to 1.0 V vs. Li/Li^+ [15], which corresponds to a theoretical capacity up to 1334 mAh/g. It is believed that the lithium ions can be stored in different defect sites of the MoS_2 depending on the morphology of the material[15]. In addition, Kartick et al. reported that MoS_2/CNT composites prepared by dry grinding method can achieve a reversible storage capacity around 1000 mAh/g[49] and X. Cao et al. reported that the MoS_2 layers grown on CVD-G has a reversible capacity above 1000 mAh/g[50]. We believe that the high capacity observed in our study is associated with the unique material structure and defect distribution of MoS_x/CNT. It worth mentioning that the MoS_x/MWNTs composites had better rate performance compared to the reported single-layer MoS_2-graphene composites[40] and much improved cycling stability than the MoS_2 electrodes[27,40]. As demonstrated by the schematical illustration image in Figure 5, the high rate capability can be attributed to the unique hierarchical nanoarchitecture of MoS_x/MWNTs which provide structural stability and transport advantages for both electrons and lithium ions. The Li^+ ion from the surrounding of MoS_x/MWNTs have sufficient contact with the Li accommodate layers, and the exposed MoS_x edges provides abundant intercalations tunnels. The MWNTs provide fast electronic conduction channels and ensure the individual high specific MoS_x layerelectrically connected during charge/discharge cycles, meanwhile the Li^+ are accommodated in the metal sulfide layers.

In conclusion, the outstanding performance of hierarchical composites based anode material is attributable to the unique synergy at the nanoscale between 1D CNT and Li^+ hosting 2D nanoseets . The CNTs provide high conductance channels and ensure the individual high specific MoS_x layerelectrically connected during charge/discharge cycles, meanwhile the Li^+ are accommodated in the metal sulfide layers. Moreover, the designed hierarchical structure with maximized surface and increased layer distance of S–Mo–S have resulted in less strain and smaller intercalation barrier of Li ions, which maintain the high lithium storage in reversible capacities, stable cycling lifetime, and excellent rate performances. Other promising applications are also anticipated to arise that take advantage of the abundant active MoS_x edges as catalysts[51–54].

Methods

Preparation of MoS_x/MWNTs nanocomposite. The multi-walled carbon nanotubes (MWNTs), L-MWNTs-60100, were purchased from Shen-zhen Nanotech Port Co., Ltd, Shenzhen, China. The $(NH4)_2MoS_4$ powder and N,N-dimethylformamide (DMF) were purchased from Sigma-Aldrich. All chemicals and raw materials were directly used without further purification. The MWNTs/MoS_2 hybrid was prepared by a solvent thermal process. In a typical experiment, 220 mg $(NH4)_2MoS_4$ powder (Sigma-Aldrich) and 100 mg MWNTs were mixed and dispersed into 30 ml of N,N-dimethylformamide (DMF) in a 40 ml Teflon autoclave. After that, the solution was sonicated at room temperature for approximately 10 mins until homogeneous solution was achieved. Then the autoclave was sealed tightly and heated at 200°C for 10 hours under autogenous pressure without intentional control of ramping and cooling rate. After cooled down to room temperature, the product was extracted by centrifugation at 10,000 rpm for 5 min. To remove the unreacted molecules and most of the DMF residuals the product was dispersed in DI water and recollected by centrifugation, this washing step was repeated for at least 5 times, the final products was MWNTs/MoS_x nano composite.

Materials characterization. X-ray photoelectron spectroscopy (XPS) analysis was performed on a KRATOS AXIS ULTRA-DLD spectrometer with a monochromatic Al $K_{\alpha 1}$ radiation ($h\nu$ = 1486.6 eV). The morphologies and microstructures of the products were characterized by transmission electron microscopy (TEM) and high resolution TEM (HRTEM) on a JEM 2100F microscope. The Raman spectra were obtained by using WITec CRM 200 confocal Raman microscopy system with a laser wavelength of 488 nm and spot size of 0.5 μm. To calibrate the wavenumber, the Si peak at 520 cm^{-1} was used as a reference.

Electrochemical measurements. The electrochemical performance of MWNTs/MoS_x nanocomposites electrode was measured with a half-cell lithium ion battery (LIBs) configuration. The 2032 coin-type cells were assembled in an argon-filled glove-box with both of the moisture and oxygen level less than 1 ppm. The working

electrode material slurry were prepared by mixing MWNTs/MoS_x, carbon black and poly(vinyldifluoride) (PVDF) at a weight ratio of 80 : 10 : 10, several drops of N-methylpyrrolidone (NMP) solvent was added into the mixture to prepare the active materials slurry. The resulting slurry was then uniformly pasted onto Ni foam , with mass loading of 4 ~ 6 mg. Lithium sheet was used as anodes and 1 M $LiPF_6$ in a 1/1 (volume ratio) mixture of ethylene carbonate (EC)/dimethyl carbonate (DMC) as electrolyte. Cegard® 2400 was used as the separator of the battery. The cells were tested on a NEWARE multi-channel battery test system with galvanostatic charge and discharge in the voltage range between 0.01 and 3.0 V vs. Li/Li^+ at various current density at room temperature. The cyclic Voltammetry (CV) and electrochemical impedance spectroscopy (EIS) were tested on an electrochemical workstation (VMP3, Bio-Logic).

1. Armand, M. & Tarascon, J. M. Building better batteries. *Nature* **451**, 652–657 (2008).
2. Cheng, F., Tao, Z., Liang, J. & Chen, J. Template-Directed Materials for Rechargeable Lithium-Ion Batteries†. *Chem Mater* **20**, 667–681 (2007).
3. Tarascon, J. M. & Armand, M. Issues and challenges facing rechargeable lithium batteries. *Nature* **414**, 359–367 (2001).
4. Etacheri, V., Marom, R., Elazari, R., Salitra, G. & Aurbach, D. Challenges in the development of advanced Li-ion batteries: a review. *Energy & Environmental Science* **4**, 3243–3262 (2011).
5. Wang, K. *et al*. Super-Aligned Carbon Nanotube Films as Current Collectors for Lightweight and Flexible Lithium Ion Batteries. *Adv Funct Mater* **23**, 846–853 (2013).
6. Venkatachalam, S. *et al*. In-Situ Formation of Sandwiched Structures of Nanotube/CuxOy/Cu Composites for Lithium Battery Applications. *ACS Nano* **3**, 2177–2184 (2009).
7. Wu, Z.-S. *et al*. Graphene Anchored with Co3O4 Nanoparticles as Anode of Lithium Ion Batteries with Enhanced Reversible Capacity and Cyclic Performance. *ACS Nano* **4**, 3187–3194 (2010).
8. Zhu, X., Zhu, Y., Murali, S., Stoller, M. D. & Ruoff, R. S. Nanostructured Reduced Graphene Oxide/Fe2O3 Composite As a High-Performance Anode Material for Lithium Ion Batteries. *ACS Nano* **5**, 3333–3338 (2011).
9. Zhang, W. *et al*. A facile approach to nanoarchitectured three-dimensional graphene-based Li–Mn–O composite as high-power cathodes for Li-ion batteries. *Beilstein Journal of Nanotechnology* **3**, 513–523 (2012).
10. Ji, H. *et al*. Ultrathin Graphite Foam: A Three-Dimensional Conductive Network for Battery Electrodes. *Nano Lett* **12**, 2446–2451 (2012).
11. Zhu, G.-N. *et al*. Binary Li4Ti5O12-Li2Ti3O7 Nanocomposite as an Anode Material for Li-Ion Batteries. *Adv Funct Mater* **23**, 640–647 (2013).
12. Liang, J., Zhao, Y., Guo, L. & Li, L. Flexible Free-Standing Graphene/SnO2 Nanocomposites Paper for Li-Ion Battery. *Acs Appl Mater Interfaces* **4**, 5742–5748 (2012).
13. Hassoun, J., Lee, K.-S., Sun, Y.-K. & Scrosati, B. An Advanced Lithium Ion Battery Based on High Performance Electrode Materials. *J Am Chem Soc* **133**, 3139–3143 (2011).
14. Hosono, E., Kudo, T., Honma, I., Matsuda, H. & Zhou, H. Synthesis of Single Crystalline Spinel LiMn2O4 Nanowires for a Lithium Ion Battery with High Power Density. *Nano Lett* **9**, 1045–1051 (2009).
15. Feng, C. *et al*. Synthesis of molybdenum disulfide (MoS2) for lithium ion battery applications. *Mater Res Bull* **44**, 1811–1815 (2009).
16. Xiao, J. *et al*. Exfoliated MoS2 Nanocomposite as an Anode Material for Lithium Ion Batteries. *Chem Mater* **22**, 4522–4524 (2010).
17. Chang, K. & Chen, W. l-Cysteine-Assisted Synthesis of Layered MoS2/Graphene Composites with Excellent Electrochemical Performances for Lithium Ion Batteries. *ACS Nano* **5**, 4720–4728 (2011).
18. Hwang, H., Kim, H. & Cho, J. MoS2 Nanoplates Consisting of Disordered Graphene-like Layers for High Rate Lithium Battery Anode Materials. *Nano Lett* **11**, 4826–4830 (2011).
19. Zhang, C., Wang, Z., Guo, Z. & Lou, X. W. Synthesis of MoS2–C One-Dimensional Nanostructures with Improved Lithium Storage Properties. *Acs Appl Mater Interfaces* **4**, 3765–3768 (2012).
20. Sen, U. K. & Mitra, S. High-Rate and High-Energy-Density Lithium-Ion Battery Anode Containing 2D MoS2 Nanowall and Cellulose Binder. *Acs Appl Mater Interfaces* **5**, 1240–1247 (2013).
21. Wang, M., Li, G., Xu, H., Qian, Y. & Yang, J. Enhanced Lithium Storage Performances of Hierarchical Hollow MoS2 Nanoparticles Assembled from Nanosheets. *Acs Appl Mater Interfaces* **5**, 1003–1008 (2013).
22. Lin, Y.-C. *et al*. Wafer-scale MoS2 thin layers prepared by MoO3 sulfurization. *Nanoscale* **4**, 6637–6641 (2012).
23. Zhan, Y., Liu, Z., Najmaei, S., Ajayan, P. M. & Lou, J. Large-Area Vapor-Phase Growth and Characterization of MoS2 Atomic Layers on a SiO2 Substrate. *Small* **8**, 966–971 (2012).
24. Shi, Y. *et al*. van der Waals Epitaxy of MoS2 Layers Using Graphene As Growth Templates. *Nano Lett* **12**, 2784–2791 (2012).
25. Liu, K. K. *et al*. Growth of Large-Area and Highly Crystalline MoS2 Thin Layers on Insulating Substrates. *Nano Letters* **12**, 1538–1544 (2012).
26. Zhou, W. *et al*. Synthesis of Few-Layer MoS2 Nanosheet-Coated TiO2 Nanobelt Heterostructures for Enhanced Photocatalytic Activities. *Small* **9**, 140–147 (2013).
27. Wang, S. *et al*. Solvothermal Synthesis of MoS2/Carbon Nanotube Composites with Improved Electrochemical Performance for Lithium Ion Batteries. *Nanoscience and Nanotechnology Letters* **4**, 378–383 (2012).
28. Ma, L., Chen, W. X., Xu, Z. D., Xia, J. B. & Li, X. Carbon nanotubes coated with tubular MoS2 layers prepared by hydrothermal reaction. *Nanotechnology* **17**, 571–574 (2006).
29. Koroteev, V. O. *et al*. Charge Transfer in the MoS2/Carbon Nanotube Composite. *The Journal of Physical Chemistry C* **115**, 21199–21204 (2011).
30. Ma, L., Chen, W.-X., Xu, Z.-D., Xia, J.-B. & Li, X. Carbon nanotubes coated with tubular MoS 2 layers prepared by hydrothermal reaction. *Nanotechnology* **17**, 571 (2006).
31. Song, X. C., Zheng, Y. F., Zhao, Y. & Yin, H. Y. Hydrothermal synthesis and characterization of CNT@MoS2 nanotubes. *Mater Lett* **60**, 2346–2348 (2006).
32. Wang, Q. & Li, J. Facilitated Lithium Storage in MoS2 Overlayers Supported on Coaxial Carbon Nanotubes. *The Journal of Physical Chemistry C* **111**, 1675–1682 (2007).
33. Baker, M. A., Gilmore, R., Lenardi, C. & Gissler, W. XPS investigation of preferential sputtering of S from MoS2 and determination of MoSx stoichiometry from Mo and S peak positions. *Appl Surf Sci* **150**, 255–262.
34. Wang, H. W., Skeldon, P. & Thompson, G. E. XPS studies of MoS2 formation from ammonium tetrathiomolybdate solutions. *Surface and Coatings Technology* **91**, 200–207 (1997).
35. Merki, D., Fierro, S., Vrubel, H. & Hu, X. Amorphous molybdenum sulfide films as catalysts for electrochemical hydrogen production in water. *Chemical Science* **2**, 1262–1267 (2011).
36. Chang, Y.-H. *et al*. Highly Efficient Electrocatalytic Hydrogen Production by MoSx Grown on Graphene-Protected 3D Ni Foams. *Adv Mater* **25**, 756–760 (2013).
37. Weber, T., Muijsers, J. C. & Niemantsverdriet, J. W. Structure of Amorphous MoS3. *J Phys Chem* **99**, 9194–9200 (1995).
38. Chang, K. & Chen, W. Single-layer MoS2/graphene dispersed in amorphous carbon: towards high electrochemical performances in rechargeable lithium ion batteries. *J Mater Chem* **21**, 17175–17184 (2011).
39. Scott, R. A. *et al*. Reactions of molybdenum trisulfide, tungsten trisulfide, tungsten triselenide, and niobium triselenide with lithium. Metal cluster rearrangement revealed by EXAFS. *Inorg Chem* **25**, 1461–1466 (1986).
40. Wang, Z. *et al*. CTAB-assisted synthesis of single-layer MoS2-graphene composites as anode materials of Li-ion batteries. *Journal of Materials Chemistry A* **1**, 2202–2210 (2013).
41. Wang, G. X., Bewlay, S., Yao, J., Liu, H. K. & Dou, S. X. Tungsten disulfide nanotubes for lithium storage. *Electrochem. Solid State Lett.* **7**, A321–A323 (2004).
42. Yang, L. *et al*. Hierarchical MoS2/Polyaniline Nanowires with Excellent Electrochemical Performance for Lithium-Ion Batteries. *Adv Mater* **25**, 1180–1184 (2013).
43. Fang, X. *et al*. Lithium storage performance in ordered mesoporous MoS2 electrode material. *Micropor Mesopor Mater* **151**, 418–423 (2012).
44. Chang, K. & Chen, W. X. L-Cysteine-Assisted Synthesis of Layered MoS2/Graphene Composites with Excellent Electrochemical Performances for Lithium Ion Batteries. *ACS Nano* **5**, 4720–4728 (2011).
45. Xiao, J. *et al*. Electrochemically Induced High Capacity Displacement Reaction of PEO/MoS2/Graphene Nanocomposites with Lithium. *Adv Funct Mater* **21**, 2840–2846 (2011).
46. Fang, X. *et al*. Mechanism of Lithium Storage in MoS2 and the Feasibility of Using Li2S/Mo Nanocomposites as Cathode Materials for Lithium–Sulfur Batteries. *Chemistry – An Asian Journal* **7**, 1013–1017 (2012).
47. Owejan, J. E., Owejan, J. P., DeCaluwe, S. C. & Dura, J. A. Solid Electrolyte Interphase in Li-Ion Batteries: Evolving Structures Measured In situ by Neutron Reflectometry. *Chem Mater* **24**, 2133–2140 (2012).
48. Chang, K. & Chen, W. In situ synthesis of MoS2/graphene nanosheet composites with extraordinarily high electrochemical performance for lithium ion batteries. *Chem Commun* **47**, 4252–4254 (2011).
49. Bindumadhavan, K., Srivastava, S. K. & Mahanty, S. MoS2-MWCNT hybrids as a superior anode in lithium-ion batteries. *Chem Commun* **49**, 1823–1825 (2013).
50. Cao, X. *et al*. Preparation of MoS2-Coated Three-Dimensional Graphene Networks for High-Performance Anode Material in Lithium-Ion Batteries. *Small,* doi:10.1002/smll.201202697 (2013).
51. Kibsgaard, J. *et al*. Cluster−Support Interactions and Morphology of MoS2 Nanoclusters in a Graphite-Supported Hydrotreating Model Catalyst. *J Am Chem Soc* **128**, 13950–13958 (2006).
52. Laursen, A. B., Kegnaes, S., Dahl, S. & Chorkendorff, I. Molybdenum sulfides-efficient and viable materials for electro - and photoelectrocatalytic hydrogen evolution. *Energy & Environmental Science* **5**, 5577–5591 (2012).
53. Bian, X. *et al*. Nanocomposite of MoS2 on ordered mesoporous carbon nanospheres: A highly active catalyst for electrochemical hydrogen evolution. *Electrochem Commun* **22**, 128–132 (2012).
54. Li, Y. *et al*. MoS2 Nanoparticles Grown on Graphene: An Advanced Catalyst for the Hydrogen Evolution Reaction. *J Am Chem Soc* **133**, 7296–7299 (2011).

Acknowledgements

This work is supported by SMART innovation grant and SUTD-ZJU research grant ZJURP1100104.

Author contributions

Y.S. and H.Y.Y. conceived the project. Y.S., Y.W. and H.Y.Y. designed and carried out research, analyzed data. Y.S. and H.Y.Y. wrote the paper. A.Y.S.T., J.I.W. and C.L.H. contributed in material characterization and discussion. Y.C.L. and L.J.L. provide scientific advice. All authors contributed to the writing and editing.

Additional information

Supplementary information accompanies this paper at http://www.nature.com/scientificreports

Competing financial interests: The authors declare no competing financial interests.

How to cite this article: Shi, Y. *et al.* Self-assembly of hierarchical MoS_x/CNT nanocomposites ($2<x<3$): towards high performance anode materials for lithium ion batteries. *Sci. Rep.* **3**, 2169; DOI:10.1038/srep02169 (2013).

This work is licensed under a Creative Commons Attribution 3.0 Unported license. To view a copy of this license, visit http://creativecommons.org/licenses/by/3.0